Supporting Information

Facile One-pot Synthesis of Sodium Ternary Chalcogenides for Energy Conversion and Storage Applications

Saeed Ahmadi Vaselabadi[a], *Brynn Benham*[a], *Colin A. Wolden*, [a, *]

[a] Chemical and Biological Engineering, Colorado School of Mines, Golden, CO

* Email: cwolden@mines.edu

Contents

Scheme S1 Standard "two-pot" Na_3SbS_4 reaction in ethanol

$$Na_2S_{(s)} \overset{ROH}{\leftrightarrow} NaHS_{(sol)} + NaOR_{(sol)} \quad \text{(S1)}$$

$$Sb_2S_{3(sol)} + 3HS^-_{(sol)} + 3OH^-_{(sol)} \rightarrow 2SbS_3^{3-}{}_{(sol)} + 3H_2O_{(l)} \quad \text{(S2)}$$

$$2SbS_3^{3-}{}_{(sol)} + 2S_{(s)} \rightarrow 2SbS_4^{3-}{}_{(sol)} \quad \text{(S3)}$$

$$3Na_2S_{(sol)} + Sb_2S_{3(sol)} + 2S_{(sol)} \overset{EtOH}{\rightarrow} 2Na_3SbS_{4(s)} \quad \text{(S4)}$$

Figure S1 Product analysis of Na_3SbS_4 one-pot reaction with chloride salt

Figure S1 displays the XRD patterns of single-step Na_3SbS_4 solution synthesis in methanol using $SbCl_3$. In the first attempt, the initial Na_3SbS_4 concentration in MeOH was set to 0.15 M, and the powder was recovered after decanting and drying the precipitate under vacuum at RT. The XRD pattern of the obtained powder shows the presence of the tetragonal phase of Na_3SbS_4. A substantial trace of NaCl was also observed in the precipitate pattern. NaCl is highly soluble in methanol (1.375 g/100 g methanol)[1], so the remaining NaCl in the precipitate could be either due to the high concentration of precursors that led to the NaCl saturation or originated from insufficient washing steps.

Repeating this reaction with a lower concentration (0.075 M) and extra washing with MeOH addresses the NaCl separation but results in a drastically low ternary yield (~34%) due to the partial solubility of Na_3SbS_4 in MeOH.[2] As a result, using a polar solvent with a comparable NaCl solubility as a washing reagent that could improve the yield while maintaining the purity of Na_3SbS_4 seemed imperative. NaCl solubility in DMSO is relatively high (0.5 g/100 g DMSO) while DMSO is expected to have a lower dissolution capability of the ternary sulfides compared to MeOH due to its lower polarity. The initial yield for $[Na_3SbS_4]$ = 0.15 M with DMSO as washing reagent is ~53% while XRD confirmed the high purity of the product. Increasing the reaction concentration improves the yield significantly; however, increases the consumption of costly DMSO washing solvent as the result rendering this system relatively inefficient in terms of processing cost and scalability (Figure S1b).

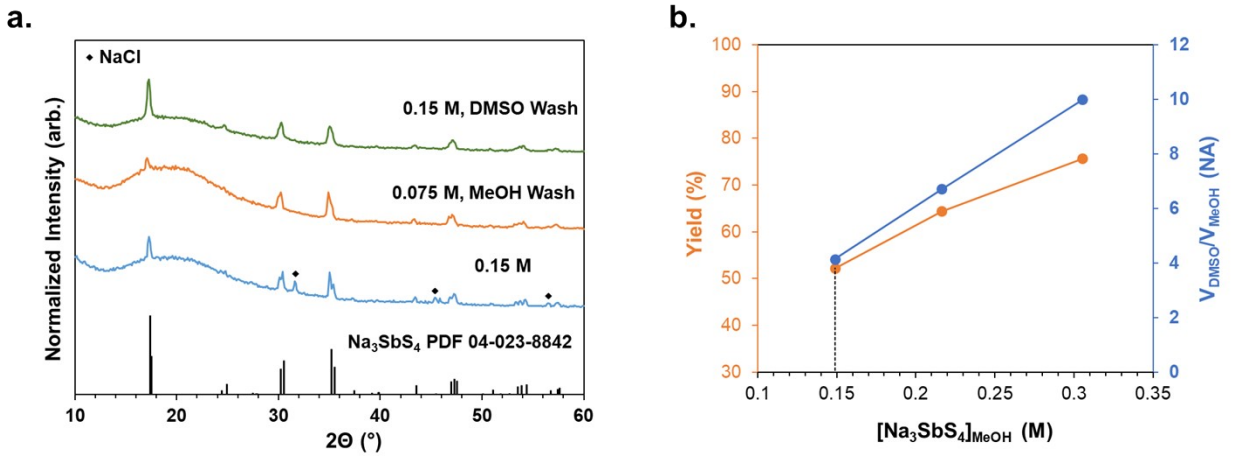

Figure S1 a. XRD patterns of Na_3SbS_4 one-pot reaction with $SbCl_3$ reagent, b. Yield and volumetric ratio of washing

solvent (DMSO) to reaction solvents (MEOH) as a function of Na_3SbS_4 initial concentration (M) in MeOH.

Figure S2 Rietveld analysis of Na_3SbS_4 one-pot reaction with bromide salt

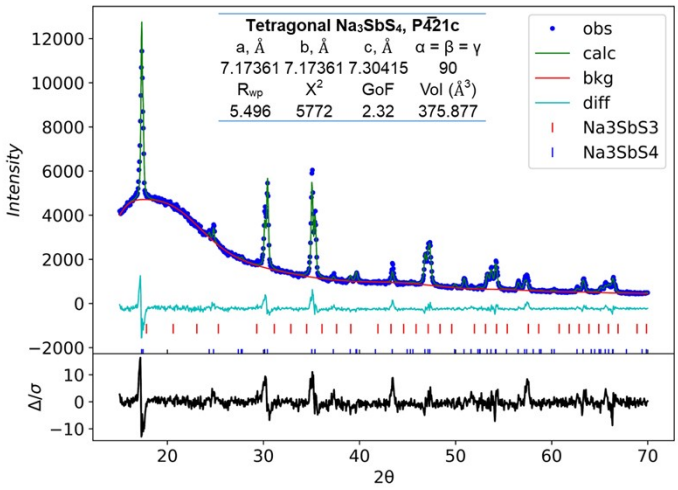

Figure S2 Rietveld refinement of Na_3SbS_4 recovered from EtOH at RT. The inset shows the lattice parameters confirm the presence of Na_3SbS_4 tetragonal phase with P421c space group.

Figure S3 Supernatant composition of Na_3SbS_4 one-pot reaction

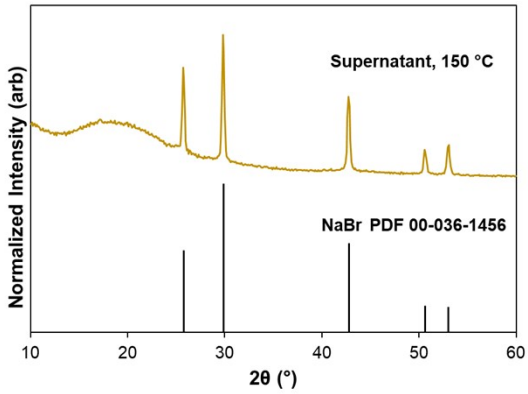

Figure S3 XRD pattern of supernatant recovered from Na_3SbS_4 one-pot reaction with bromide halide.

Figure S4 EDAX analysis of Na_3SbS_4

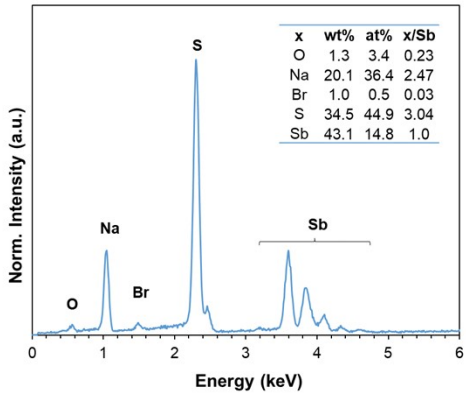

Figure S4 EDAX spectrum of one-pot Na_3SbS_4 recovered at RT.

Figure S5 FTIR analysis of Na_3SbS_4

We used FTIR spectroscopy to identify any possible impurities from the obtained ternary sulfide. Figure S5 compares the IR spectra of RT and 150 °C with pure Na_2S reagent and recovered Na_2S from EtOH solution. Small traces of organic residues (C-H and O-H bonds) observed in the RT sample from the ethanolic solution are mostly removed after the mild heat treatment at 150 °C. The lack of major peaks from precipitated ethanolic Na_2S indicates that most of the NaHS and EtONa formed from Na_2S dissolution are either consumed in the reaction or removed during washing steps. Since the stoichiometric amount of Na_2S is sufficient to produce highly pure ternary sulfide with a considerable yield (~92-95%), we can assume that NaHS is the dominant reactive species in the Na_2S solution

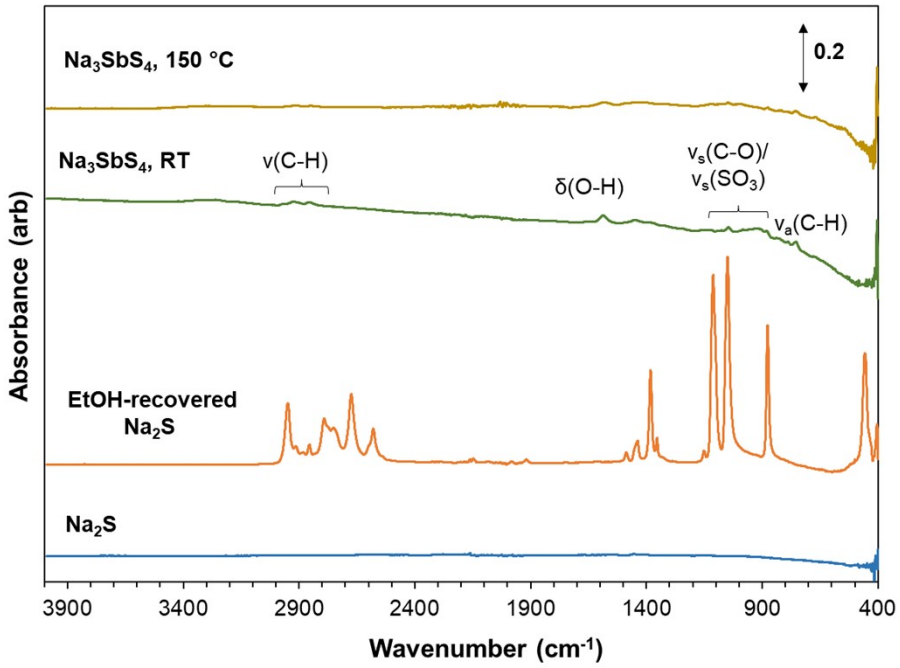

Figure S5 FTIR spectra of Na_3SbS_4 recovered from the one-pot reaction with bromide salt at RT and dried at 150 °C compared with Na_2S reagent and its ethanolic solution products.

Scheme S2 Standard "two-pot" Na_3SbSe_4 reaction in ethanol

$$Se_{(s)} + NaBH_{4(sol)} + 3C_2H_5OH_{(l)} \rightarrow NaHSe_{(sol)} + B(OC_2H_5)_3 + 3H_{2\,(g)} \quad \text{(S5)}$$

$$6NaHSe_{(sol)} + 2SbCl_{3\,(sol)} \rightarrow Sb_2Se_{3\,(s)} + 3NaCl_{(sol)} + 3HCl_{(sol)} \quad \text{(S6)}$$

$$3NaHSe_{(sol)} + Sb_2Se_{3\,(s)} + 3NaOH_{(sol)} + 2Se \rightarrow 2Na_3SbSe_{4\,(s)} + 3H_2O \quad \text{(S7)}$$

Scheme S3: Possible decomposition reactions in ethanolic Se solutions

$$2NaHSe_{(sol)} + B(OC_2H_5)_{3\,(sol)} + 3H_2O_{(l)} \rightarrow Na_2Se_{2\,(sol)} + H_3BO_{3\,(sol)} + 3C_2H_5OH_{(l)} + H_{2\,(sol)} \quad \text{(S8)}$$

$$Na_2Se_{2\,(sol)} + 2H_2O_{(l)} \rightarrow Se^0_{(s)} + 2NaOH_{(sol)} + 5H_{2\,(g)} \quad \text{(S9)}$$

$$Na_2Se_{2(sol)} \xrightarrow{O_2} Na_2Se_{(sol)} + Se^0_{(s)} \quad \text{(S10)}$$

Figure S6 XRD analysis of Na_3SbSe_4 one-pot supernatant

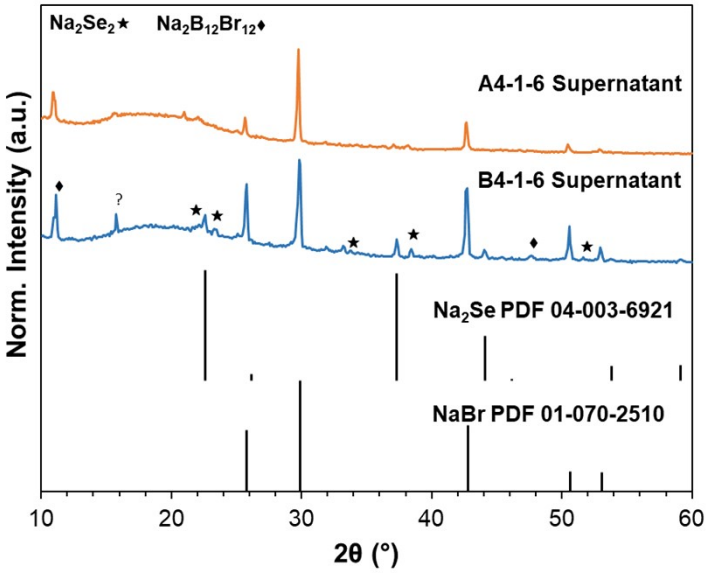

Figure S6 XRD patterns of supernatant from A4-2-6 and B4-2-6 samples. Supernatant powders are obtained after drying at 120 °C under Ar flow.

Figure S7 Raman analysis of Na_3SbSe_4 one-pot products

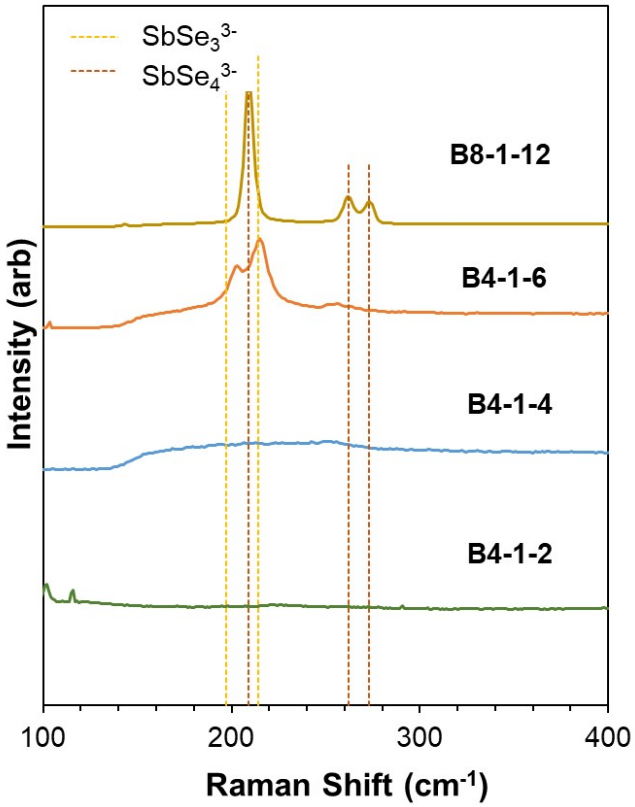

Figure S7 Raman spectra of Na_3SbSe_4 precipitates recovered at RT from colorless Se solution (B).

We conducted Raman analysis to determine various molecular bonding in selenide products of solution B. The 100-400 cm^{-1} region was probed as it is the range of interest for selenide compounds. The spectra from B4-1-2 and B4-1-4 samples do not show any peaks correlated to Raman active vibrational modes of ternary selenide. Alternatively, vibrational modes of $SbSe_4^{3-}$ and $SbSe_3^{3-}$ units are observed in the product recovered from the B4-1-6 reaction. The bands at 205 and 214 cm^{-1} are assigned to stretching modes of [$SbSe_3$] indicating a red shift compared to the spectrum of single crystals of Na_3SbSe_3 possibly due to a change in the molecular environment of the mixed ternary phase and the presence of unremoved solvated molecules.[3,4] The bands at 209, 262, and 273 are attributed to stretching modes of $SbSe_4$ polyanions.[5,6] In complete agreement with the diffraction results, the B8-1-12 product exhibits pure $SbSe_4$ polyanions without any other impurities.

Figure S8 Na_3SbSe_4 reaction using Na_2Se_2 precursor

To probe the applicability of Na_2Se_2 as a Se source in the ternary selenides' synthesis, we used a Se solution precursor mostly containing Se_2^{2-} anions in ethanol. For this reaction, an ethanolic solution of Na_2Se_2 (Figure S8a) was produced by the reduction of Se with $NaBH_4$ in the presence of sodium ethoxide[7] which was further reacted with $SbBr_3$ and NaOH with [Se]: [Sb]: [NaOH] = 4: 1: 6 stoichiometry as detailed in the Experimental Section. XRD pattern of the recovered product (Figure S7b) shows a major Na_3SbSe_4 phase with a minor $NaSbSe_2$ phase implying the possibility of ternary reaction with only diselenide anions.

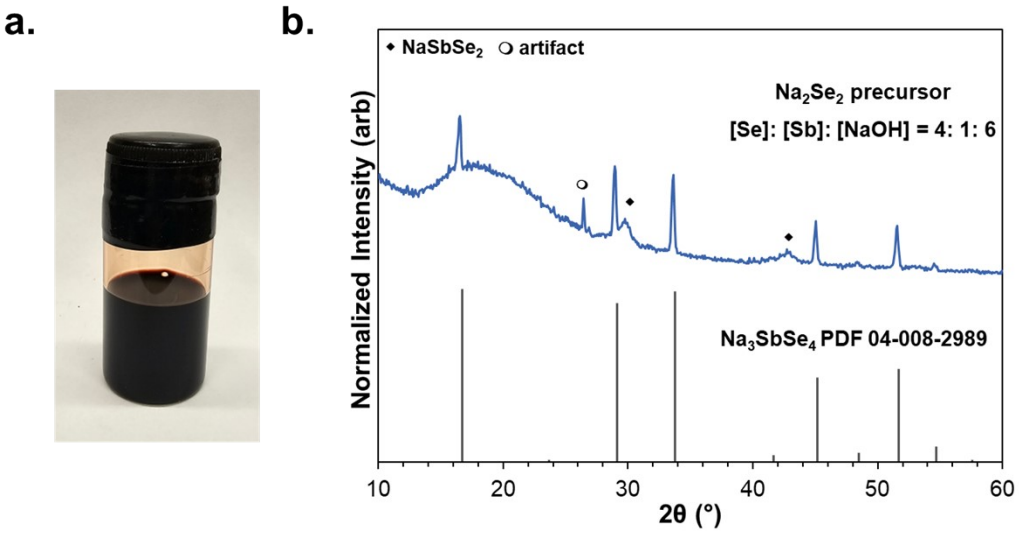

Figure S8 a. Photograph of Na_2Se_2 solution in ethanol. b. XRD pattern of product from Na_2Se_2 reaction with $SbBr_3$ and NaOH using [Se]: [Sb]: [NaOH] = 4: 1: 6 stoichiometry.

Figure S9 XRD analysis of Na_3SbSe_4 reaction with no basic agent.

In these reactions, we observed that NaOH plays a crucial role in forming the desired 314 phase. The excess of NaOH promotes the oxidation of antimony from (III) state in $NaSbSe_2$/Na_3SbSe_3 to the (V) state in Na_3SbSe_4. The oxidation of Sb (III) to Sb (V) requires simultaneous reduction of certain species in the system to maintain the charge neutrality. Herein, we can assume the reduction of Se_2^{2-} to Se_2. in the absence

of H_2 evolution is the key factor that results in the oxidation of Sb (III) to Sb(V). Interestingly, a ternary reaction with no NaOH resulted in a highly pure $NaSbSe_2$ further demonstrating the role of the basic agent in the oxidation of Sb (Figure S9).

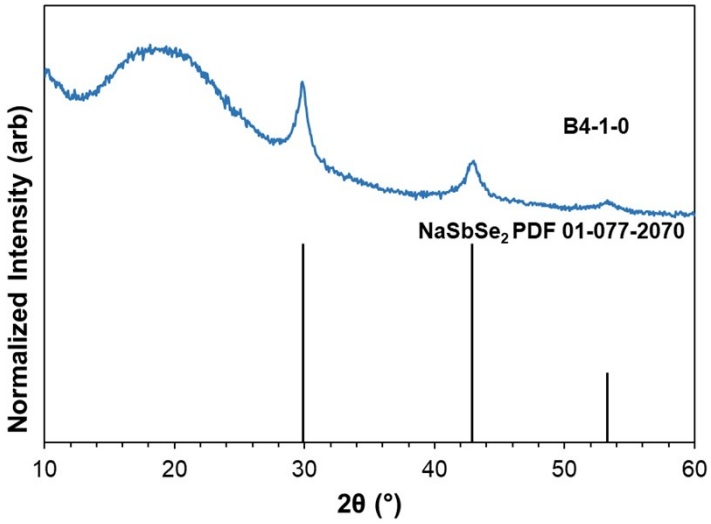

Figure S9 XRD patterns of ternary reaction precipitate with no basic agent added (B4-1-0): [NaHSe]: [Sb]: [NaOH] = 4: 1: 0 in EtOH recovered at RT.

Figure S10 Lattice structure of Na_3SbSe_4

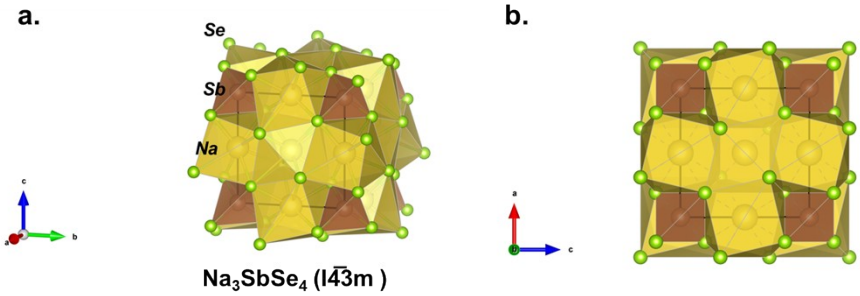

Figure S10 a. The crystal lattice structure of Na_3SbSe_4, b. projected along the b-axis.

Figure S11 EDAX Mapping of Na_3SbSe_4

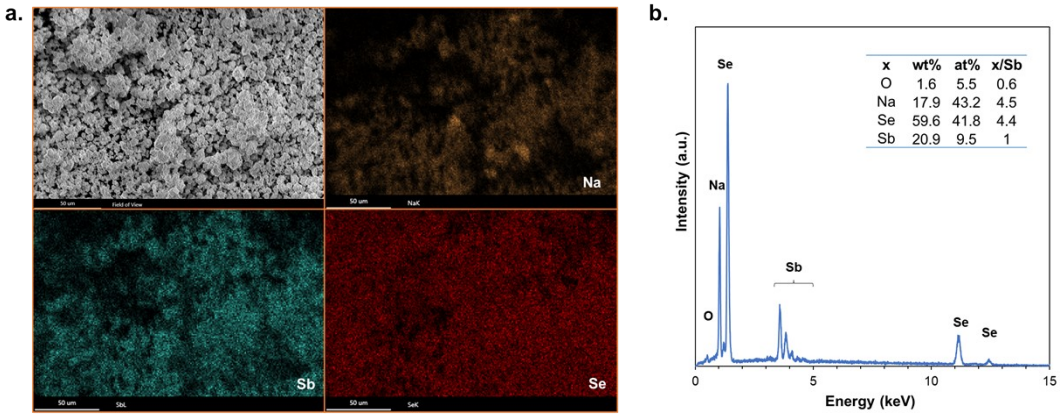

Figure S11 a. SEM micrograph and EDAX elemental mapping of A8-1-12 sample. b. corresponding elemental composition of the Na_3SbSe_4 sample recovered from EtOH at RT.

Figure S12 FTIR analysis of RT and heat-treated Na_3SbSe_4

The IR spectra of Na_3SbSe_4 recovered at RT and later annealed at 200 °C compared with pure EtOH signal. Most organic residues (C-H and O-H bonds) observed in the RT sample from the ethanolic solution are removed even though small traces of oxyselenide species at low wavenumbers are still present.

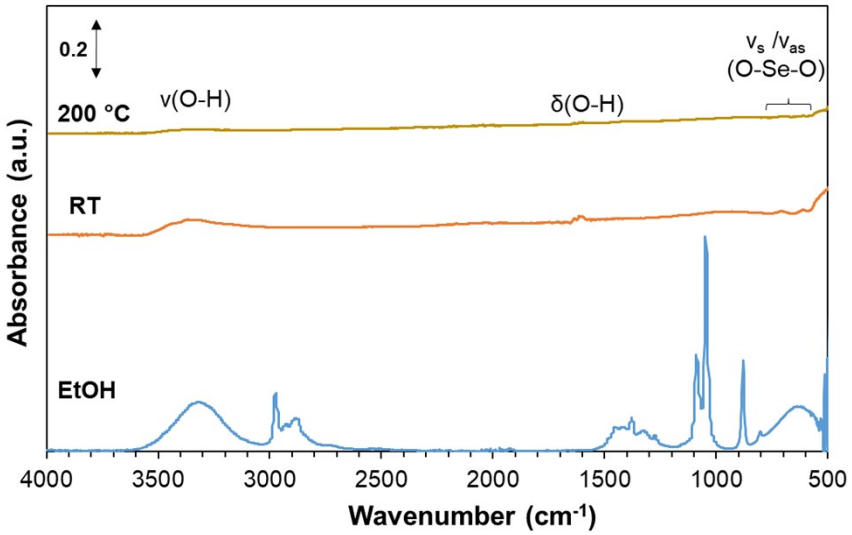

Figure S12 FTIR spectra of Na_3SbSe_4 dried at RT and 200 °C compared with pure ethanol IR scan.

Figure S13 Electronic conductivity of Na_3SbCh_4.

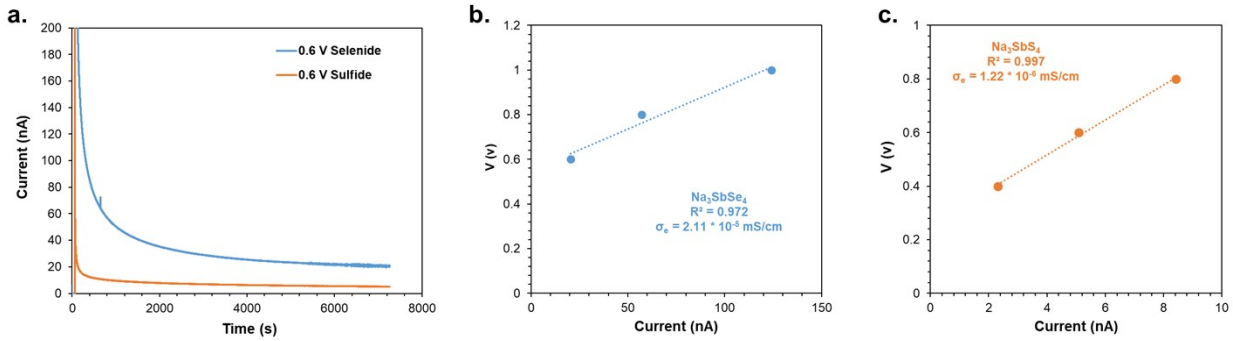

Figure S13 a. DC polarization curves of Na_3SbCh_4 (Ch = S, Se) at 0.6 V. Electronic conductivity of b. Na_3SbS_4, and c. Na_3SbSe4 calculated from Ohm's law.

Figure S14 Raman analysis of $NaSbS_2$

Raman spectra of the RT and annealed $NaSbS_2$ samples are shown in Figure S14. The change in intensity and position of Raman peaks can provide useful information about the local structure of chemical bonding, relative change in order/disorder, and orientation of crystalline compounds.[8] The number of major Raman peaks observed here matches with the Medina-Gonzalez et al.[9] report; however, the peak positions at ~287 and ~ 317 cm^{-1} are slightly different from the $NaSbS_2$ synthesized using the colloidal approach possibly due to differences in local structure induced by different synthesis methods and post-processing. The rise in intensity and narrowing of the observed peaks in the RT sample upon heat treatment/further indicates the structural phase change in $NaSbS_2$ and higher local order in monoclinic polymorph.

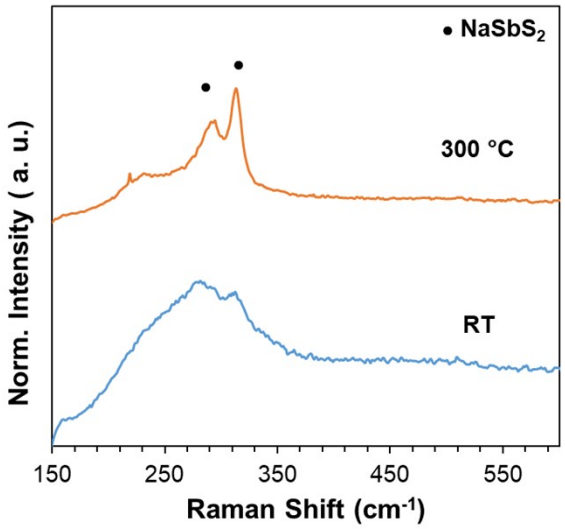

Figure 14 Raman spectra of $NaSbS_2$ before and after annealing at 300 °C.

Figure S15 Morphological analysis of $NaSbS_2$

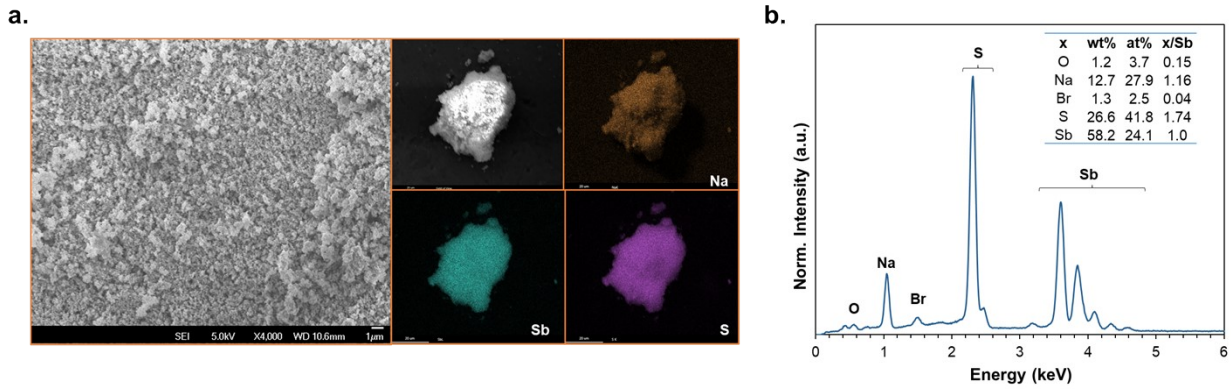

Figure S15 SEM and EDAX mapping of $NaSbS_2$ recovered from the "one-pot" reaction in EtOH at RT.

Figure S16 XRD and EDAX analysis of one-pot $NaSbSe_2$

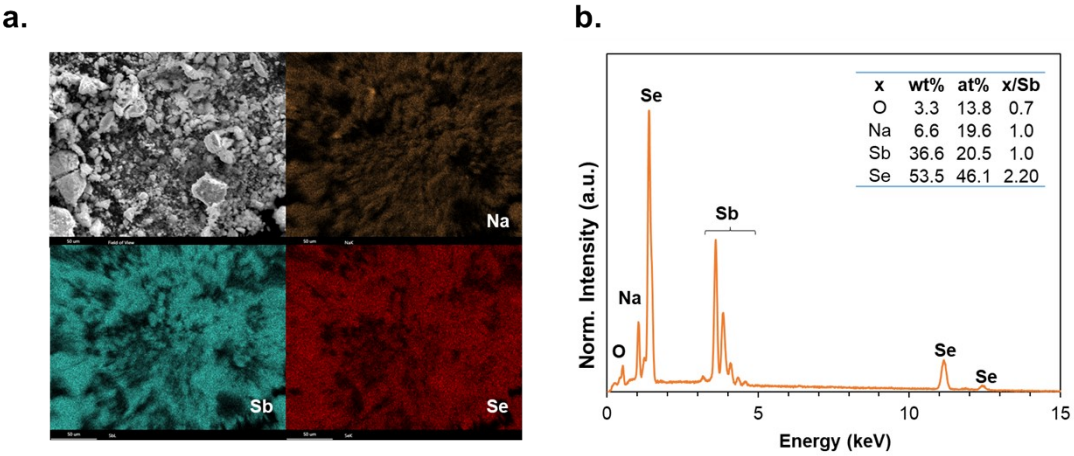

Figure S16 a. EDAX mapping, and b. corresponding elemental composition of $NaSbSe_2$ powder annealed at 300 °C.

$NaBiCh_2$ (Ch= S, Se) Synthesis and Structural Characterization

To date, $NaBiCh_2$ (Ch = S, Se) has been synthesized using hydrothermal[10–12], colloidal solution[13–15], and high-temperature sintering[16] approaches. Even though binary chalcogenides exist in various crystal structures and offer different physiochemical properties, ternary chalcogenides offer additional degrees of freedom in adjusting their properties and performance for a given application; however, that also adds more complexity to the synthesis. Specifically, one of the challenging aspects in multinary chalcogenide synthesis is the tendency to form binary chalcogenide phases.[14,17,18] In this context, Bi_2S_3 is the main impurity formed in the hydrothermal synthesis of $NaBiS_2$.[12,19]

Our initial attempts to extend the one-pot approach to Bi-based materials resulted in a mixed binary and ternary phase as depicted in Figure S16a. However, the excess of sulfur and NaOH proved to stabilize the ternary phase while improving the crystallinity of the RT-recovered sample. Figure 8a compares the XRD profiles of reaction products with an excess of NaOH ([Na_2S]: [Bi]: [NaOH] =2: 1: 5, denoted as NBS2-1-

5) or without NaOH (NBS2-1-0) and excess of both Na_2S and NaOH (NBS5-1-5). The RT product of the NBS2-1-0 sample is almost amorphous while the sample with excess NaOH shows broad peaks matching with cubic ($Fm\bar{3}m$) $NaBiS_2$. NBS5-1-5 exhibits the highest crystallinity recovered at RT indicating the impact of sulfur concentration on crystal growth. Annealing at 300 °C does not significantly change the crystallinity of pure $NaBiS_2$ in the NBS5-1-5 reaction. In cases of NBS2-1-0 and 2-1-5 results in a mixture of Bi, binary, and ternary sulfide, highlighting the impact of alkaline conditions in stabilizing the ternary compound. Bismuth salts such as $Bi(NO_3)_3$ and $BiCl_3$ are reported to go through strong hydrolysis in aqueous solutions, decreasing the pH and neutralizing available alkali species. Hence, excess alkaline presence is needed to neutralize the formed acidity.[19,20] We presume excess Na_2S/NaOH provides a similar impact in the ethanolic solution of Na_2S and $BiBr_3$ by creating an alkaline condition that ultimately improves the solubility of intermate Bi_2S_3 and facilitates its reaction to generate $NaBiS_2$. Additionally, it improves the crystal growth of ternary chalcogenides.

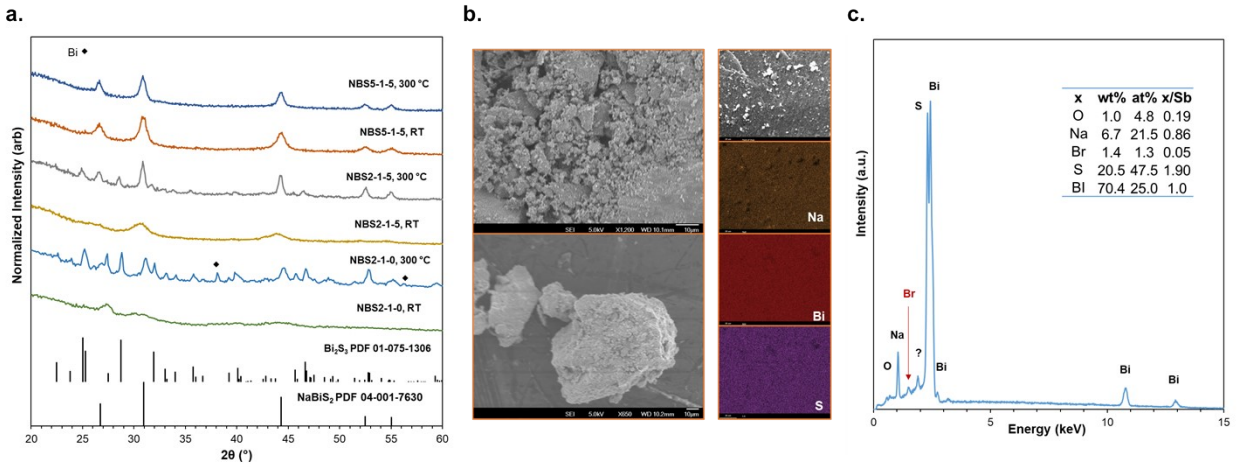

Figure S17 a. XRD patterns of NaBiS2 products with different [Na_2S]: [Bi]:[OH] concentrations. b. SEM micrograph, EDAX mapping, and c. the corresponding composition of $NaBiS_2$ annealed at 300 °C (NBS5-1-5, 300 °C).

SEM micrograph of annealed $NaBiS_2$ shows micron-sized agglomerates of various shapes (Figure 16a). It is important to note that size and morphology control in this reaction scheme is quite difficult without the use of any surfactant or capping agents. EDAX mapping and corresponding elemental composition (Figure 16c, d) exhibit a homogenous elemental distribution with Na/Bi = 0.86, and S/Bi = 1.90 molar ratios very close to the expected stoichiometric values. There is a small trace of bromine possibly from unremoved NaBr present despite vigorous H_2O washing in the purification process.

Our efforts to synthesize $NaBiSe_2$ through similar concentration tuning of precursors resulted in a mixed phase of Bi_2Se_3 and $NaBiSe_2$ (Figure S18). Additional studies utilizing other precursors or adjusting pH conditions are needed to optimize the reaction conditions and obtain pure selenide compounds.

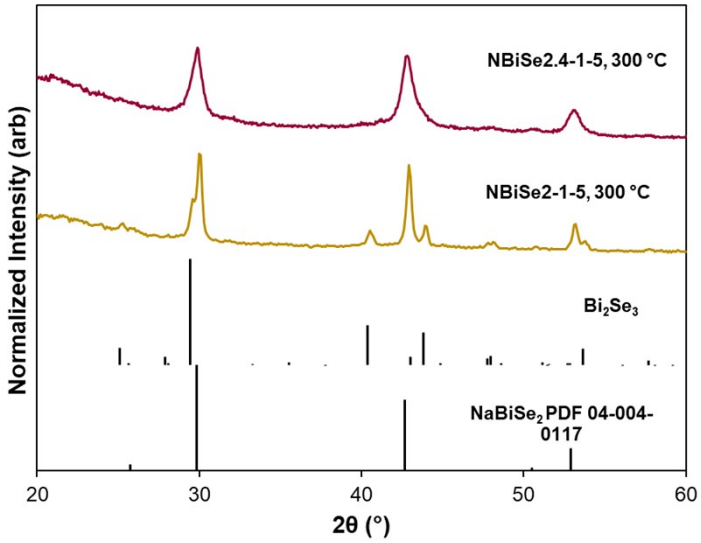

Figure S18 XRD patterns of $NaBiSe_2$ recovered from ethanol solution with various [Se]:[Bi]:[OH ratios.

Table S1 Fitting results of EIS spectra of synthesized Na_3SbCh_4.

Effective capacitance is calculated from the Brug equation[21]: $C_{eff} = Q^{1/n} R^{\frac{1-n}{n}}$

Sample	R_1 (Ω)	Q_1 (S/s^n)	n_1	C_1 (F)	Q_2 (S/s^n)	n_2
Na_3SbS_4	180.7	6.71E-6	0.31	1.96E-12	4.21E-7	0.87
Na_3SbSe_4	672.3	6.39E-7	0.55	1.09E-9		

Table S2 Summary of solution-phase synthesis of ternary chalcogenides

Sample	Chalcogen precursor (Conc.)	Pnictogen precursor (Conc.)	NaOH (Conc.)	Solvent	Recovery temperature (°C)	Product
Chloride-based NSbS (0.15 M)	Na_2S (0.45 M), S (0.15 M)	$SbCl_3$ (0.15 M)	0	MeOH-DMSO	RT	Na_3SbS_4 (97.8%), NaSbS2 (2.2%)
Bromide-based NSbS	Na_2S (0.3M), S (0.1 M)	$SbBr_3$ (0.1 M)	0	EtOH	RT, 150 °C	Na_3SbS_4, $NaSbS_2$
$NaSbS_2$ ($Fm\bar{3}m$)	Na_2S (0.2 M)	$SbBr_3$ (0.1 M)	0	EtOH	RT	$NaSbS_2$
$NaSbS_2$ (C2/c)	Na_2S (0.24 M)	$SbBr_3$ (0.1 M)	0	EtOH	300 °C	$NaSbS_2$
NBS2-1-0	Na_2S (0.2 M)	$BiBr_3$ (0.1 M)	0	EtOH	RT, 300 °C	Bi_2S_3 (major), $NaBiS_2$ (major), Bi (trace)

NBS2-1-5	Na_2S (0.2 M)	$BiBr_3$ (0.1 M)	0.5 M	EtOH	RT, 300 °C	$NaBiS_2$ (major), Bi_2S_3 (minor)
NBS5-1-5	Na_2S (0.5 M)	$BiBr_3$ (0.1 M)	0.5 M	EtOH	RT, 300 °C	$NaBiS_2$
$NaSbSe_2$	Colorless Se (0.22 M)	$SbBr_3$ (0.11 M)	0.44 M	EtOH	RT, 300 °C	$NaSbSe_2$
NBiSe2-1-5	Colorless Se (0.2 M)	$BiBr_3$ (0.2M)	0.4 M	EtOH	300 °C	$NaBiSe_2$, Bi_2Se_3(trace)
NBiSe2.4-1-5	Colorless Se (0.24 M)	$BiBr_3$ (0.2M)	0.4 M	EtOH	300 °C	$NaBiSe_2$, Bi_2Se_3(trace),

Table S3 Summary of synthesis parameters and performance reports of Na_3SbCh_4 (Ch= S, Se) in the literature.

Ternary SSE	**Synthesis method**	**Precursors**	**P_{fab} (MPa)**	**Heat-treatment (°C)**	**σ_{Na+} (mS/cm)**	**E_a (eV)**	**Ref.**
Na_3SbS_4	Hydrate Purification	$Na_3SbS_4.9H_2O$	320	150	1	0.22	[22]
Na_3SbS_4	Solid-state	Na_2S, Sb_2S_3, S	370	550	1.10	0.20	[2]
	Dissolution-precipitation (MeOH, H_2O)			500	0.23	0.37	
Na_3SbS_4	Solution (H_2O)	Na_2S, Sb_2S_3, S	370	200	0.15	0.35	[23]
Na_3SbS_4	Solution (H_2O)	Na_2S, Sb_2S_3, S	150	720	1.2	0.24	[24]
Na_3SbS_4	Solution (H_2O)	$Na_2S.9H_2O$, Sb_2S_3, S	140	350	0.12	-	[25]
Na_3SbS_4	Solid-state	Na_2S, Sb_2S_3, S	600	-	0.98	0.17	[26]
Na_3SbS_4	Solid-state	Na, Sb, S	700	400	1.9	-	[27]
Na_3SbS_4	Solution (H_2O)	Na_2S, Sb_2S_3, S	150	570	0.35	0.34	[28]
Na_3SbSe_4	Solid-state	Na, Sb, Se	650	100	0.85	0.193	[29]
Na_3SbSe_4	Solid-state	Na, Sb, Se	700	300	3.7	0.19	[6]
Na_3SbSe_4	Solution (EtOH)	Se, $NaBH_4$ Sb_2Se_3, NaOH	275	200	0.25	0.11	[30]

Na_3SbSe_4	Solution (EDA-PT)	Na, Se, Sb_2Se_3,	275	300	0.175	0.14	[30]
Na_3SbS_4	Solution (EtOH)	Na_2S, $SbBr_3$, SnS_2, S	275	RT	0.38	0.19	This work
Na_3SbSe_4	Solution (EtOH)	Se, $NaBH_4$, $SbBr_3$, NaOH		RT	0.17	0.21	

References

1 S. P. Pinho and E. A. Macedo, Solubility of NaCl, NaBr, and KCl in water, methanol, ethanol, and their mixed solvents, *J Chem Eng Data*, 2005, **50**, 29–32.

2 A. Banerjee, K. H. Park, J. W. Heo, Y. J. Nam, C. K. Moon, S. M. Oh, S.-T. T. Hong and Y. S. Jung, Na3SbS4: A Solution Processable Sodium Superionic Conductor for All-Solid-State Sodium-Ion Batteries, *Angewandte Chemie - International Edition*, 2016, **55**, 9634–9638.

3 C. Pompe and A. Pfitzner, Na3SbSe3: Synthesis, crystal structure determination, raman spectroscopy, and ionic conductivity, *Z Anorg Allg Chem*, 2012, **638**, 2158–2162.

4 H. J. Breunig, S. Güleç, B. Krebs and M. Dartmann, Synthesis and Structure of (MeSe)3Sb, *Zeitschrift für Naturforschung B*, 1989, **44**, 1351–1354.

5 N. Ding, Y. Takabayashi, P. L. Solari, K. Prassides, R. J. Pcionek and M. G. Kanatzidis, Cubic gyroid frameworks in mesostructured metal selenides created from tetrahedral Zn 2+, Cd 2+, and in 3+ ions and the [SbSe 4] 3- precursor, *Chemistry of Materials*, 2006, **18**, 4690–4699.

6 N. Wang, K. Yang, L. Zhang, X. Yan, L. Wang and B. Xu, Improvement in ion transport in Na3PSe4–Na3SbSe4 by Sb substitution, *J Mater Sci*, 2018, **53**, 1987–1994.

7 X. Yang, Q. Wang, Y. Tao and H. Xu, A Modified Method to Prepare Diselenides by the Reaction of Selenium with Sodium Borohydride, *J Chem Res*, 2002, **2002**, 160–161.

8 G. Gouadec and P. Colomban, Raman Spectroscopy of nanomaterials: How spectra relate to disorder, particle size and mechanical properties, *Progress in Crystal Growth and Characterization of Materials*, 2007, **53**, 1–56.

9 A. M. Medina-Gonzalez, P. Yox, Y. Chen, M. A. S. Adamson, B. A. Rosales, M. Svay, E. A. Smith, R. D. Schaller, K. Wu, A. J. Rossini, K. Kovnir and J. Vela, Solution-Grown Ternary Semiconductors: Nanostructuring and Stereoelectronic Lone Pair Distortions in I–V–VI 2 Materials, *Chemistry of Materials*, 2022, **34**, 7357–7368.

10 S. Kang, Y. Hong and Y. Jeon, A facile synthesis and characterization of sodium bismuth sulfide (NaBiS2) under hydrothermal condition, *Bull Korean Chem Soc*, 2014, **35**, 1887–1890.

11 P. Rong, S. Gao, H. Lu, S. Ren, M. Zhang, S. Jiao, Y. Zhang and J. Wang, Hierarchical Nanosheet-Based NaBiS2 Flowers for High-Performance and Self-Powered Broadband Photodetectors, *ACS Appl Nano Mater*, 2022, **5**, 11003–11010.

12 H. Fei, Z. Feng and X. Liu, Novel sodium bismuth sulfide nanostructures: a promising anode materials for sodium-ion batteries with high capacity, *Ionics (Kiel)*, 2015, **21**, 1967–1972.

13 B. A. Rosales, M. A. White and J. Vela, Solution-Grown Sodium Bismuth Dichalcogenides: Toward Earth-Abundant, Biocompatible Semiconductors, *J Am Chem Soc*, 2018, **140**, 3736–3742.

14 N. Kapuria, B. Nan, T. E. Adegoke, U. Bangert, A. Cabot, S. Singh and K. M. Ryan, Colloidal Synthesis of Multinary Alkali-Metal Chalcogenides Containing Bi and Sb: An Emerging Class of I–V–VI 2 Nanocrystals with Tunable Composition and Interesting Properties, *Chemistry of Materials*, 2023, **35**, 4810–4820.
15 C. Yang, Z. Wang, Y. Wu, Y. Lv, B. Zhou and W. H. Zhang, Synthesis, characterization, and photodetector application of alkali metal bismuth chalcogenide nanocrystals, *ACS Appl Energy Mater*, 2019, **2**, 182–186.
16 A. Baqais, N. Tymińska, T. Le Bahers and K. Takanabe, Optoelectronic Structure and Photocatalytic Applications of Na(Bi,La)S 2 Solid Solutions with Tunable Band Gaps, *Chemistry of Materials*, 2019, **31**, 3211–3220.
17 C. Behera, R. Samal, C. S. Rout, R. S. Dhaka, G. Sahoo and S. L. Samal, Synthesis of CuSbS2 Nanoplates and CuSbS2-Cu3SbS4 Nanocomposite: Effect of Sulfur Source on Different Phase Formation, *Inorg Chem*, 2019, **58**, 15291–15302.
18 C. Coughlan, M. Ibáñez, O. Dobrozhan, A. Singh, A. Cabot and K. M. Ryan, Compound Copper Chalcogenide Nanocrystals, *Chem Rev*, 2017, **117**, 5865–6109.
19 H. Wang, Z. Xie, X. Wang and Y. Jia, NaBiS2 as a Novel Indirect Bandgap Full Spectrum Photocatalyst: Synthesis and Application, *Catalysts*, 2020, **10**, 413.
20 H. Wang, J. Ding, H. Xu, L. Qiao, X. Wang and Y. Lin, One-Pot Synthesis of BiCuSO Nanosheets under Ambient Atmosphere as Broadband Spectrum Photocatalyst, *Nanomaterials*, 2019, **9**, 540.
21 G. J. Brug, A. L. G. van den Eeden, M. Sluyters-Rehbach and J. H. Sluyters, The analysis of electrode impedances complicated by the presence of a constant phase element, *Journal of Electroanalytical Chemistry*, 1984, **176**, 275–295.
22 H. Wang, Y. Chen, Z. D. Hood, G. Sahu, A. S. Pandian, J. K. Keum, K. An and C. Liang, An Air-Stable Na3SbS4 Superionic Conductor Prepared by a Rapid and Economic Synthetic Procedure, *Angewandte Chemie - International Edition*, 2016, **55**, 8551–8555.
23 T. W. Kim, K. H. Park, Y. E. Choi, J. Y. Lee and Y. S. Jung, Aqueous-solution synthesis of Na3SbS4 solid electrolytes for all-solid-state Na-ion batteries, *J Mater Chem A Mater*, 2018, **6**, 840–844.
24 S. Yubuchi, A. Ito, N. Masuzawa, A. Sakuda, A. Hayashi and M. Tatsumisago, Aqueous solution synthesis of Na3SbS4–Na2WS4 superionic conductors, *J Mater Chem A Mater*, 2020, **8**, 1947–1954.
25 H. Cao, M. Yu, L. Zhang, Z. Zhang, X. Yan, P. Li and C. Yu, Stabilizing Na3SbS4/Na interface by rational design via Cl doping and aqueous processing, *J Mater Sci Technol*, 2021, **70**, 168–175.
26 W. Weng, G. Liu, Y. Li, L. Shen and X. Yao, Tungsten and oxygen co-doped stable tetragonal phase Na3SbS4 with ultrahigh ionic conductivity for all-solid-state sodium batteries, *Appl Mater Today*, 2022, **27**, 101448.
27 L. Li, R. Xu, L. Zhang, Z. Zhang, M. Yang, D. Liu, X. Yan and A. Zhou, O-Tailored Microstructure-Engineered Interface toward Advanced Room Temperature All-Solid-State Na Batteries, *Adv Funct Mater*, , DOI:10.1002/adfm.202203095.
28 H. Gamo, N. H. H. Phuc, H. Muto and A. Matsuda, Effects of Substituting S with Cl on the Structural and Electrochemical Characteristics of Na3SbS4Solid Electrolytes, *ACS Appl Energy Mater*, 2021, **4**, 6125–6134.
29 S. Xiong, Z. Liu, H. Rong, H. Wang, M. McDaniel and H. Chen, Na3SbSe4-xSx as Sodium

Superionic Conductors, *Sci Rep*, 2018, **8**, 2–8.
30 S. A. Vaselabadi, K. Palmer, W. H. Smith and C. A. Wolden, Scalable Synthesis of Selenide Solid-State Electrolytes for Sodium-Ion Batteries, *Inorg Chem*, 2023, **62**, 17102–17114.